Generating and identifying optical orbital angular momentum with silicon photonic circuits

Jie Sun,[1],* Michele Moresco,[1] Gerald Leake,[2] Douglas Coolbaugh,[2] and Michael R. Watts[1]

[1]*Research Laboratory of Electronics, Massachusetts Institute of Technology, Cambridge, Massachusetts 02139, USA*

[2]*College of Nanoscale Science and Engineering, University at Albany, Albany, New York 12203, USA*

Corresponding author: sunjie@mit.edu

Here, we propose and demonstrate a silicon nanophotonic phased array that is capable of generating light carrying optical orbital angular momentum (OAM). Optical beams carrying different orbital angular momenta have been generated. In addition, the generated OAM wavefronts are experimentally identified by interfering with another on-chip generated Gaussian beam, opening up opportunities of integrating conventional optical systems and functionalities on to a silicon chip.   © 2014 Optical Society of America

OCIS codes: (130.3120) Integrated optics devices; (250.3140) Integrated optoelectronic circuits; (280.5110) Phased-array radar.

http://dx.doi.org/10.1364/OL.39.005977

Optical vortices, whose electrical field has angular phase dependence, i.e., $E \sim \exp(j \cdot l \cdot \theta)$, carry an orbital angular momentum (OAM) $l \cdot \hbar$ per photon in the beam-propagation direction, where θ is the azimuthal angle with respect to the beam axis and the l-value represents the OAM state, which is usually but not necessarily an integer [1,2]. Light-carrying OAM has found many applications, such as in optical communications where the spatially orthogonal OAM states are utilized to provide another multiplexing dimension in order to further increase the data capacity of optical communication systems [3,4], as well as in optical micromanipulations where the OAM of the photons can be directly transferred to that of an optically trapped particle causing it to rotate [5,6]. OAM beams also generate Doppler frequency shifts when interacting with rotating objects, providing a means for measuring rotation speed [7]. In addition to these classical applications, OAM is also widely used in quantum information processing to create high-dimensional quantum entanglement [8–10].

A variety of methods have been utilized to generate optical OAM beams, mainly with free-space approaches, such as a spiral phase plate [11], liquid-crystal-based spatial light modulators [6], and plasmonic metasurfaces [12]. Alternatively, generating OAM beams with integrated optics is of great interest for device miniaturization, enhanced stability, and the potential to integrate with other on-chip photonic components and functionalities. Indeed, several integrated OAM generators have been demonstrated, including a complex photonic integrated circuit based on star couplers [13] and a compact microring resonator OAM emitter [14]. Recently, we have demonstrated a large-scale silicon photonic integrated circuit, i.e., the optical phased array [15], which has shown remarkable accuracy in controlling the optical phase and hence is well-suited to generate optical OAM beams. Here we demonstrate the generation of optical beams with various OAM states using rectilinear nanophotonic phased arrays. In addition, to identify these OAM states, the wavefront of the generated light is visualized by interfering with a Gaussian beam generated on the same chip, as an example of integrating conventional

free-space optical systems on to a compact silicon chip using photonic integrated circuits.

Previously we have shown that optical phased arrays can be used to accurately engineer the optical wavefront by coding the phase of individual antennas in the array accordingly [15]. The capability to accurately control the phase of each antenna can also be used here to generate OAM beams. As illustrated by Fig. 1(a), each optical antenna in a 16×16 phased array emits with a phase ϕ determined by its angular position, i.e., $\phi = l \cdot \theta$, where θ is the azimuthal angle of the antenna with respect to the center of the array and the OAM state l equals 3 in Fig. 1(a). Note that some antennas in the phase array are not present in order to make the array circularly symmetric so that the optical intensity is uniform along the azimuthal direction. The designed OAM phased array was fabricated in a 300-mm silicon-on-insulator (SOI) process using 193-nm optical immersion lithography, where the device layer of 220 nm was used to form the waveguide and optical antennas. Figure 1(b) shows the scanning-electron micrograph (SEM) of the fabricated OAM-phased array consisting of 180 optical antennas. The antenna spacing is 9 μm, which is a multiple of the operating wavelength (1.55 μm). The phase emitted by the antennas is passively adjusted to emit with the phase pattern shown in Fig. 1(a), in a way similar to that described in [15] by use of waveguide delay lines before each antenna. Transverse-electric (TE) polarized light at 1.55 μm was coupled into the silicon bus waveguide and the optical power was then distributed two-dimensionally using directional couplers with varied lengths along the bus waveguide to uniformly feed the antennas. Figure 1(c) shows the measured near-field emission of the OAM phased array, where uniform emission from all 180 nanoantennas was observed, highlighting the robustness of the design and the accuracy of the silicon photonic fabrication. The 180 optical nanoantennas interfere in the far field to create the OAM beam. Figures 1(d) and 1(e) show the simulated and measured far-field pattern, where annular beam patterns are seen in the far field with zero intensity in the center, which is a signature of the optical OAM beam because the phase is undefined
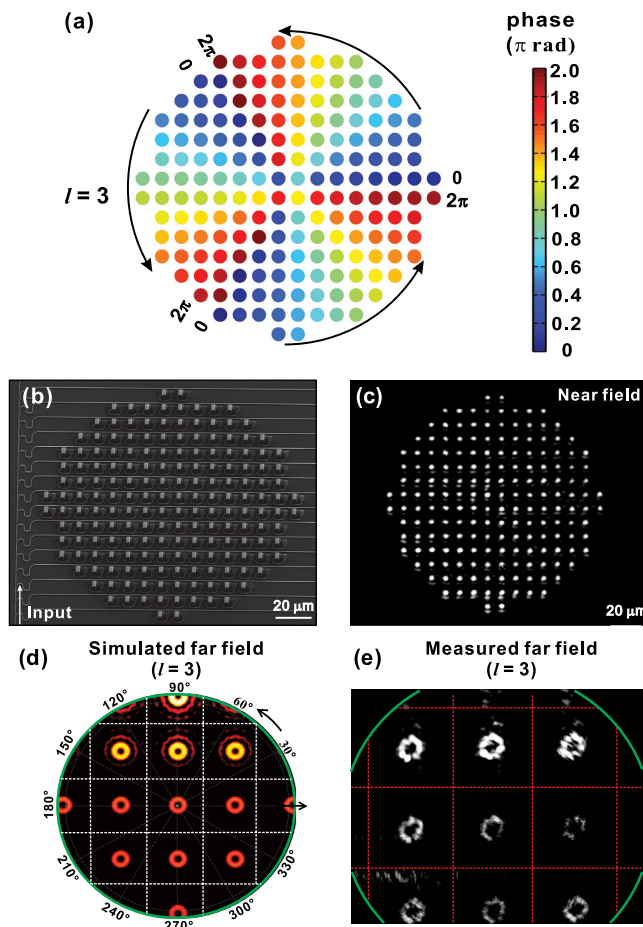
Fig. 1.   (a) Phase profile of a 16×16 optical phased array to generate an $l = 3$ optical OAM beam. (b) An SEM of the fabricated 16×16 phased array. (c) The measured near-field emission of the OAM phased array. (d) The simulated and (e) measured far-field image of the OAM phased array where multiple interference orders are seen.
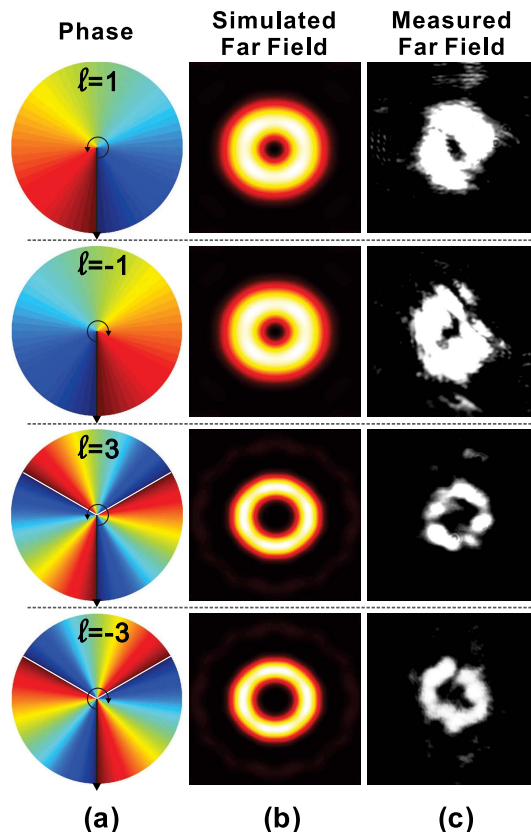

Fig. 2.   (a) Phase profile of the OAM beam with OAM states $l = \pm 1$ and $l = \pm 3$. (b) The simulated and (c) measured far-field pattern of OAM beams with different states generated by the phased arrays.

in the center of the beam. In Fig. 1(e), it can be seen that multiple interference orders were generated in the far field due to the antenna spacing being larger than a half wavelength. While it is generally desirable to emit just a single order, multiple OAM beams can be used, for example, to simultaneously trap and rotate multiple particles in optical micromanipulation. It is also noted that there is intensity variation in the interference orders where the orders in the upper row [Figs. 1(d) and 1(e)] have the highest intensity, because the optical antenna emits more toward the upper part of the image [15]. By coding the OAM phased array with different angular phase profiles, optical beams with different OAM states can be generated accordingly. As shown in Fig. 2, optical beams with OAM state $l = \pm 1$ and $l = \pm 3$ were created in the far field with the signature annular pattern. Note that only one interference order is shown in Fig. 2.

As shown in Fig. 2, OAM beams with different states look almost the same except that the higher-order OAM beams have a bigger zero-intensity region in the center. In order to further identify the state, or the l-value, of an OAM beam, one needs to reveal the helical wavefront of the beam. A common technique to visualize the wavefront of an optical beam is to interfere it with a

reference beam whose wavefront is already known. As illustrated in Figs. 3(a) and 3(c), when an OAM beam interferes with a copropagating Gaussian beam, a spiral interference pattern is generated [16], as shown in Figs. 3(b) and 3(d). The OAM state l is then identified by the number of arms in the spiral, while the sign of the OAM state is revealed by the handedness or chirality of the spiral pattern. This technique is widely used to observe the OAM beams, mainly using conventional free-space interference setups where a Gaussian reference beam is created and combined with the OAM beam through some free-space optics [12,14]. However, the free-space interference generally requires high mechanical and environmental stability since the interference pattern is sensitive to the relative phase between the two interfering beams. Fortunately, with the aide of optical phased arrays, the conventional free-space interference setup can also be integrated on a silicon photonic chip to generate stable interference patterns without using any free-space optics. As shown in Fig. 4(a), a 32×32 phased array was first designed to generate the Gaussian reference beam by simultaneously engineering both the phase and the amplitude of the optical antennas, as demonstrated in [17]. Then a smaller array, designed to generate an OAM beam, was superimposed with the Gaussian array in the center [in the red circle in Fig. 4(a)] to form a single optical phased array, by adjusting the directional couplers to achieved the desired amplitude emission profile and by adjusting the waveguide delay
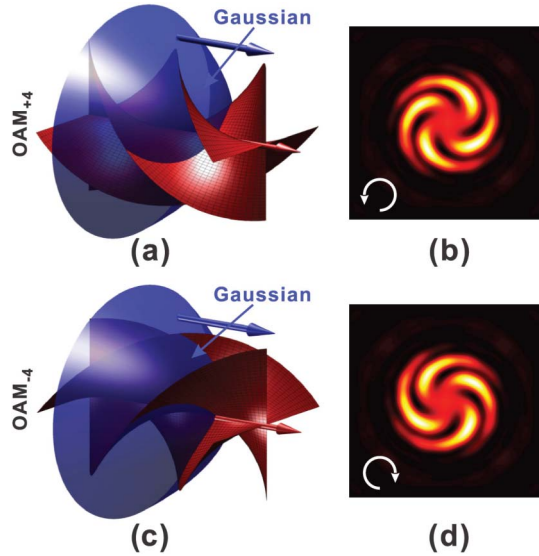
Fig. 3. (a) Illustration of an $l = +4$ OAM beam interfering with a Gaussian reference beam. (b) The interference pattern with four spiral arms and right-hand chirality corresponding to $l = +4$. (c) Illustration of an $l = -4$ OAM beam interfering with a Gaussian reference beam. (d) The interference pattern with four spiral arms and left-hand chirality corresponding to $l = -4$.
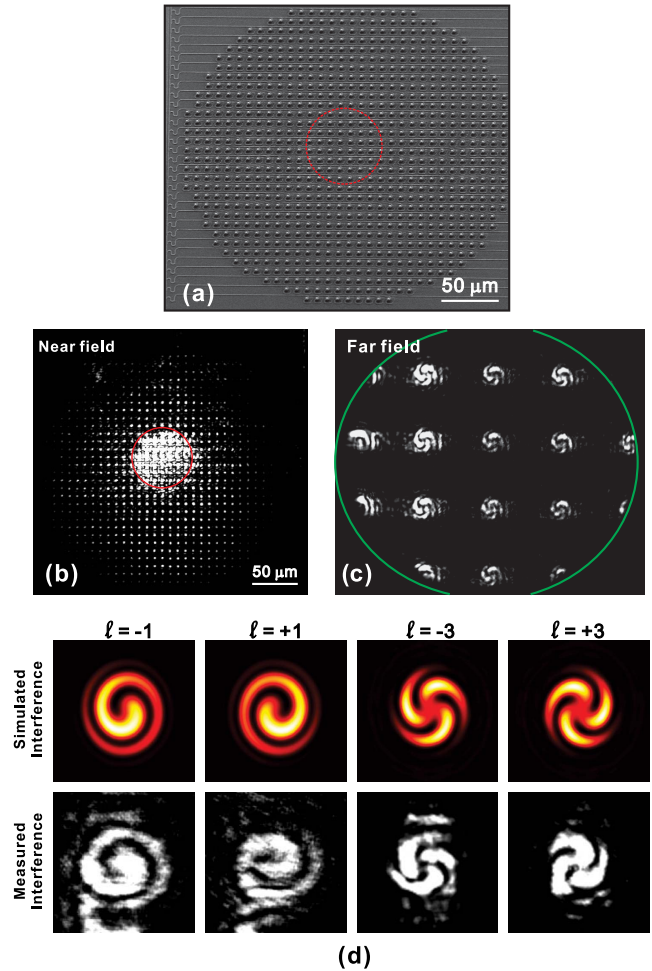

Fig. 4. (a) SEM of a Gaussian phased array superimposed with an OAM phased array in the center. (b) The measured near-field emission of the superimposed phased array. (c) The measured far field of the superimposed phased array. (d) The interference pattern of the Gaussian reference beam with different OAM beams $l = \pm 1$ and $l = \pm 3$, generated by the superimposed phased arrays.

lines for the required phase emission profile. Figure 4(b) shows the measured near field when light is coupled into the waveguide to excite all of the optical antennas in the array. It can be seen that the center of the array is much brighter since the Gaussian array overlaps with the OAM array in the red circle. The generated Gaussian beam and the OAM beam copropagate in free space and interfere with each other in the far field to create the spiral interference pattern, as shown in Fig. 4(c), where an $l = 3$ OAM beam interferes with the Gaussian reference beam to create the signature spiral pattern with three arms. Since no free-space optical component is involved here, and the two beams, generated from the same chip, always share the same optical path, the resulting interference pattern is stable and not affected by mechanical or environmental perturbations. Similarly, Fig. 4(d) shows the interference patterns of the Gaussian reference beam with different OAM beams $l = \pm 1$ and $l = \pm 3$.

In conclusion, we have demonstrated integrated silicon photonic optical phased arrays to generate OAM beams with a variety of states, which opens up opportunities to conveniently use integrated OAM generators for wide-ranging applications, such as communication, quantum information, sensing, and optical micromanipulation. By leveraging the state-of-the-art silicon photonic integration capability, higher-order OAM beams with high mode purity can be achieved by incorporating more optical antennas to form very large-scale arrays [15]. Further, it also highlights the capability of silicon photonic integrated circuits in generating complex optical beamforms. Moreover, the conventional free-space interference system was fully integrated on a silicon chip to identify the different OAM states, as an example of replacing conventional bulk optical systems with photonic integrated circuits, a goal of photonic integration. These demonstrations show that complex optical functionalities can now be realized in a compact silicon chip with unprecedented complexity and accuracy, holding promise for applications such as light detection and ranging and optical coherence tomography, etc.

References
1. L. Allen, M. W. Beijersbergen, R. J. C. Spreeuw, and J. P. Woerdman, Phys. Rev. A **45**, 8185 (1992).
2. M. Padgett, J. Courtial, and L. Allen, Phys. Today **57**(5), 35 (2004).
3. J. Wang, J. Yang, I. M. Fazal, N. Ahmed, Y. Yan, H. Huang, Y. Ren, Y. Yue, S. Dolinar, M. Tur, and A. E. Willner, Nat. Photonics **6**, 488 (2012).
4. N. Bozinovic, Y. Yue, Y. Ren, M. Tur, P. Kristensen, H. Huang, A. E. Willner, and S. Ramachandran, Science **340**, 1545 (2013).
5. J. E. Curtis and D. G. Grier, Phys. Rev. Lett. **90**, 133901 (2003).

6. V. Garcés-Chávez, D. McGloin, M. J. Padgett, W. Dultz, H. Schmitzer, and K. Dholakia, Phys. Rev. Lett. **91**, 093602 (2003).
7. M. P. J. Lavery, F. C. Speirits, S. M. Barnett, and M. J. Padgett, Science **341**, 537 (2013).
8. A. Mair, A. Vaziri, G. Weihs, and A. Zeilinger, Nature **412**, 313 (2001).
9. J. Leach, B. Jack, J. Romero, A. K. Jha, A. M. Yao, S. Franke-Arnold, D. G. Ireland, R. W. Boyd, and S. M. Barnett, Science **329**, 662 (2010).
10. A. Nicolas, L. Veissier, L. Giner, E. Giacobino, D. Maxein, and J. Laurat, Nat. Photonics **8**, 234 (2014).
11. J. Leach, E. Yao, and M. Padgett, New J. Phys. **6**, 71 (2004).
12. N. Yu, P. Genevet, M. A. Kats, F. Aieta, J. Tetienne, F. Capasso, and Z. Gaburro, Science **334**, 333 (2011).
13. C. R. Doerr, N. K. Fontaine, M. Hirano, T. Sasaki, L. L. Buhl, and P. J. Winzer, *Proceedings of the European Conference on Optical Communications* (Optical Society of America, 2011), paper Th.13.A.3.
14. X. Cai, J. Wang, M. J. Strain, B. Johnson-Morris, J. Zhu, M. Sorel, J. L. O'Brien, M. G. Thompson, and S. Yu, Science **338**, 363 (2012).
15. J. Sun, E. Timurdogan, A. Yaacobi, E. S. Hosseini, and M. R. Watts, Nature **493**, 195 (2013).
16. N. Yu, P. Genevet, F. Aieta, M. A. Kats, R. Blanchard, G. Aoust, J. Tetienne, Z. Gaburro, and F. Capasso, IEEE J. Sel. Top. Quantum Electron. **19**, 4700423 (2013).
17. J. Sun, E. S. Hosseini, A. Yaacobi, D. B. Cole, G. Leake, D. Coolbaugh, and M. R. Watts, Opt. Lett. **39**, 367 (2014).